Journal of Physics: Conference Series

PAPER • **OPEN ACCESS**

Optical, structural, morphological and chemical properties of doped TiO_2 nanoparticles with $FeCl_3$

To cite this article: Cátia Afonso *et al* 2022 *J. Phys.: Conf. Ser.* **2407** 012001

View the article online for updates and enhancements.

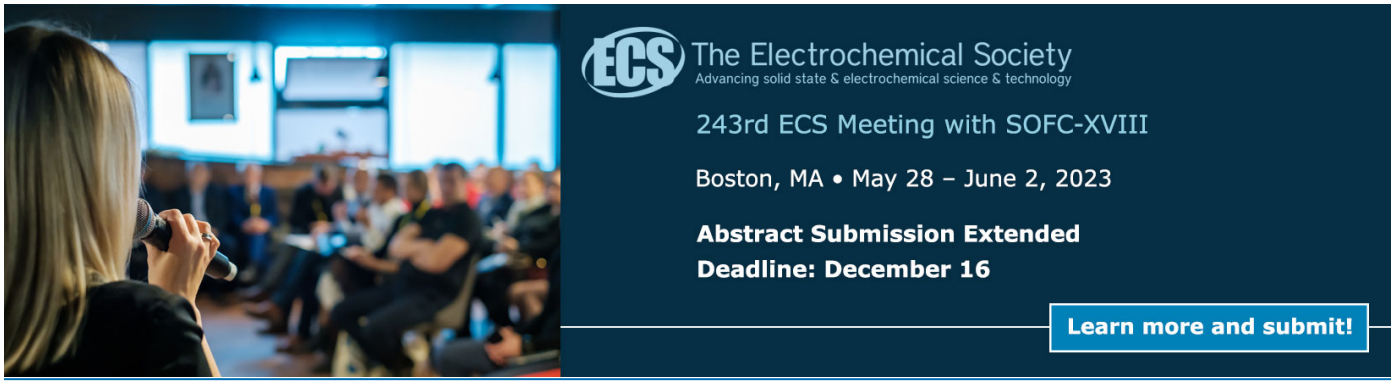

This content was downloaded by mfcosta@ from IP address 188.250.82.82 on 14/12/2022 at 16:03

Optical, structural, morphological and chemical properties of doped TiO_2 nanoparticles with $FeCl_3$

Cátia Afonso[1*], Iran Rocha Segundo[1,2*], Orlando Lima Jr.[2], Salmon Landi Jr. [3], Natália Homem[4], Manuel F. M. Costa[5], Elisabete Freitas[2] and Joaquim Carneiro[1*]

[1] Centre of Physics of Minho and Porto Universities (CF-UM-UP), University of Minho, Azurém Campus, Guimarães, Portugal;
[2] ISISE, Department of Civil Engineering, University of Minho, Guimarães, Portugal;
[3] Federal Institute Goiano, Rio Verde, Brazil;
[4] Digital Transformation CoLab (DTx), Building 1, Campus of Azurém, University of Minho, Guimarães, Portugal;
[5] Centre of Physics of Minho and Porto Universities (CF-UM-UP), Gualtar Campus, University of Minho, Braga, Portugal

[*]catiaj_afonso@hotmail.com; iran_gomes@hotmail.com; carneiro@fisica.uminho.pt

Abstract. To achieve high photocatalytic activity, TiO_2 nanoparticles nanoparticles require an excitation source in ultraviolet radiation. Incorporating chemical elements into the TiO_2 lattice can tune its band gap, resulting in an edge-shifted red absorption to reduce energies, improving photocatalytic performance in the visible region of the electromagnetic spectrum. In this research, TiO_2 semiconductor nanoparticles were subjected to a doping process using iron chloride ($FeCl_3$) powder to activate photocatalysis under visible light and consequently improve pollutant capture. To study the effectiveness of the doping process, the main ratios (1:1), (1:1.622) and (1:3) of TiO_2:$FeCl_3$ were evaluated using Diffuse Reflectance Spectroscopy (DRS), X-ray diffraction (XRD), Fourier-Transform Infrared Spectroscopy (FTIR) and Scanning Electron Microscopy (SEM). The main results of this research show that doping TiO_2 with $FeCl_3$ shifted the absorption edge to longer wavelength values, changing the optical properties of the material and decreasing the band gap (E_g) of TiO_2 compared to the undoped TiO_2 (reference). There are no relevant differences between the XRD pattern of the samples with TiO_2-$FeCl_3$ and TiO_2 nanoparticles (reference). The fraction of the anatase phase in doped TiO_2 nanoparticles has the same magnitude as the reference TiO_2. Regarding FTIR, the Fe-doping process alters the TiO_2 reference spectrum, increasing the intensity of hydroxyl bonds and peaks particularly, indicating the Ti-O-Fe bond vibration.

Keywords: band gap energy, semiconductor nanoparticles, diffuse reflectance, nano-TiO_2, photocatalysis

Content from this work may be used under the terms of the Creative Commons Attribution 3.0 licence. Any further distribution of this work must maintain attribution to the author(s) and the title of the work, journal citation and DOI.
Published under licence by IOP Publishing Ltd

1. Introduction

Titanium dioxide (TiO_2), is one of the most studied semiconductor materials due to characteristics such as its optical and electronic properties, chemical stability, availability, low cost and non-toxicity. Due to its redox photocatalytic properties, this semiconductor allows the degradation of harmful gases when activated by ultraviolet (UV) radiation. [1–5].

For photocatalysis to occur, there must be an acceleration of a chemical reaction including photocatalyst substances, such as TiO_2 nanoparticles. When boosted by light irradiation, energy levels higher than their band gap energy must be obtained. Usually, the existing semiconductors, such as TiO_2, Fe_2O_3, ZnO, CeO_2, and others, are some of those selected as photocatalysts because of their higher band gap energy (E_g) and because of their distinct electronic structure, i.e., unoccupied conduction band and occupancy band [5,6].

The sunlight is mostly composed of visible and infrared photons, with only 3%–5% of the UV range [4,7,8]. To overcome this, research is still necessary on TiO_2 particles doping to decrease its E_g to the wavelength range of visible light [4,9,10].

One way to decrease the band gap energy of nanoparticles is by doping processes. These processes suppress (e^-/h^+) pair recombination by electron/hole trapping [5]. Since, TiO_2 exhibits a high band energy value (>3 eV), it requires high absorption of photons with energy in the ultraviolet region of the electromagnetic spectrum to be activated, forming -OH soporiferous groups and photocatalytic activity [5,11–13].

Metal and non-metal doping of TiO_2 has proven to be an effective way to improve photocatalytic properties. Aiming outdoor applications, the doping process opens up the possibility to change their electronic structure of nano-TiO_2, thus modifying their optical properties and chemical composition [11,12]. The incorporation of metal ions, such as nickel, chromium, iron, vanadium, and zinc in the TiO_2 doping process is reported in the literature [12].

The incorporation of iron (Fe^{3+}), become sensitive to the TiO_2 doping process to visible light and a major advantage of their inclusion is their potential application in photocatalysis, due to the reduction of the energy gap and consequently, increase the absorption efficiency of visible light [12,14]. Thus, it is essential the use doped-TiO_2 and improve the process to produce photocatalytic treatments for outdoor applications to maximise the photodegradation efficiency [7,15,16].

This research work aims to evaluate the process of doping TiO_2 nanoparticles with iron chloride ($FeCl_3$) to activate photocatalysis under visible light. The structure, morphological, optical and chemical properties of $FeCl_3$-doped TiO_2 powders were investigated using Diffuse Reflectance Spectroscopy (DRS), X-ray Diffraction (XRD), Fourier-Transform Infrared Spectroscopy (FTIR) and Scanning Electron Microscopy (SEM).

2. Material and Methods

The semiconductor nanoparticles were subjected to a doping process using iron (Fe^{3+}). Initially, a suspension solution of TiO_2 was prepared in 100 mL of distilled water, and an aqueous solution containing various concentrations of $FeCl_3$ in 100 mL of distilled water. Then both mixtures were blended and kept under stirring at 70 °C for 150 min. Afterwards, these dispersions were filtered through filter paper and then washed successively with distilled water. Finally, after obtaining the filtered material, the remaining material from the filter was dried in an oven at 60 °C for 12 h.

The concentrations of TiO_2 and $FeCl_3$ were varied in order to obtain the best conditions:(1:1), (1:1.622) and (1:3). Thus, the samples were named by their TiO_2-$FeCl_3$ proportions. For example, (1:1.1622) means that this sample was prepared with the concentration of 1 g/100 mL of TiO_2 and 1.1622 g/100 mL of $FeCl_3$, respectively.

To study the doping effectiveness, the main variations of doped TiO_2 were characterized. Initially, the band gap of the semiconductor nanoparticles was analyzed using Diffuse Reflectance Spectroscopy (DRS) and Kubelka-Munk transform in order to determine the optical band gap energy (E_g). Subsequently, X-ray diffraction (XRD) was used to identify the crystalline phase of each doped material.

Fourier-Transform Infrared Spectroscopy (FTIR) was performed to analyze the chemical composition of the doped materials (presence and chemical bonds) and finally, Scanning Electron Microscopy (SEM) was analyzed to investigate the homogenization and dispersion of the doped samples at the various concentrations.

2.1 Reduction of the semiconductor's band gap

Light absorption measurements were performed to determine information about the concentrations of reference TiO_2 (undoped) and the various concentrations of doped TiO_2-$FeCl_3$. Then, reflectance spectroscopy tests were performed with diffuse UV-Vis reflectance spectroscopy. Unlike the transmittance parameter for liquids, reflectance on solid surfaces is quite advantageous for quantifying the quality of reflected light. To measure light adsorption, it can be determined by a parameter called the Kubelka-Munk function, F(R) [17]:

$$F\,(R) = \frac{(1-R)^2}{2R} = \frac{\alpha}{S'} \tag{1}$$

where R corresponds to the reflectance, and α and S are, respectively, the absorption and scattering coefficients.

The coefficient α is correlated to the incident photon energy, $E = \left(\frac{1239.7}{\lambda}\right)$ [18], according to Tauc's equation, where λ corresponds to the wavelength. The band gap is calculated from the Kubelka–Munk transform $[F(R) \times E]^{1/2}$.

2.2 X-ray diffraction (XRD)

The TiO_2 powders doped with $FeCl_3$ were analyzed by X-ray diffraction using a CuKα radiation source of a Philips PW 1710 X-ray diffractometer with the purpose of studying the crystalline phase of the doped materials at various concentrations.

2.3 *Scanning Electron Microscopy (SEM)*

The morphology of the doped materials was analyzed through Scanning Electron Microscopy (SEM) images. It aimed to verify whether $FeCl_3$ had been incorporated into the TiO_2 through the doping process. In this way, it was possible to obtain a magnification of about 200,000× at a 500 nm wavelength. Its high-vacuum resolution was about 10 kV with through-less detector (TLD) in secondary electron (SE) mode. In this analysis, the working distance (WD) is about 5 mm. In general, the shorter the WD, the higher the achievable resolution. The horizontal field width (HFW) clearly defines the scale of the image, and it is especially useful when the image is reduced or enlarged. In these figures the HFW was about 1.49 μm.

2.4 Fourier-Transform Infrared Spectroscopy (FTIR)

FTIR was used to analyze the chemical composition of the samples, i.e., to verify which chemical bonds exist in the doping of TiO_2 with $FeCl_3$. The chemical groups of the doped materials were compared with undoped TiO_2 (reference) and undoped $FeCl_3$ (reference) from a Shimadzu IR-Prestige-21 spectrometer (Kyoto, Japan) with a spectral range of 400 cm^{-1} to 4000 cm^{-1}.

3. Results and Discussion

3.1 *Diffuse Reflectance Spectroscopy (DRS)*

Through Diffuse Reflectance Spectroscopy (DRS) it is possible to obtain the relation reflectance versus wavelength of the doped material, and by the Kubelka-Munk function to obtain the absorbance of each material doped with different concentrations of $FeCl_3$ and the undoped TiO_2 (reference).

As can be seen in Figure 1 and Figure 2, the results of undoped TiO_2 indicate that there is strong photoabsorption only at wavelengths below 400 nm (i.e., in the UV radiation). Due to the presence of iron, the doped TiO_2 for any concentrations showed a shift of the absorption edge to longer wavelengths (i.e. red shift). These results clearly show that the doping process with $FeCl_3$ promoted changes in the optical properties of the material.

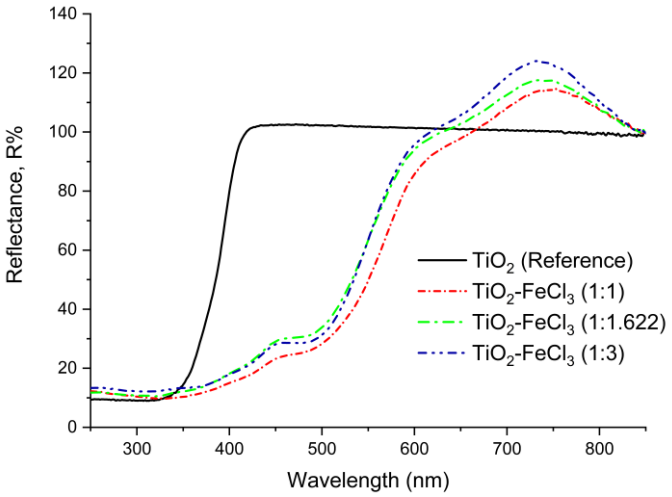

Figure 1- Results of reflectance versus wavelength for the undoped TiO_2 (reference) and doped TiO_2 with $FeCl_3$ with the different concentrations.

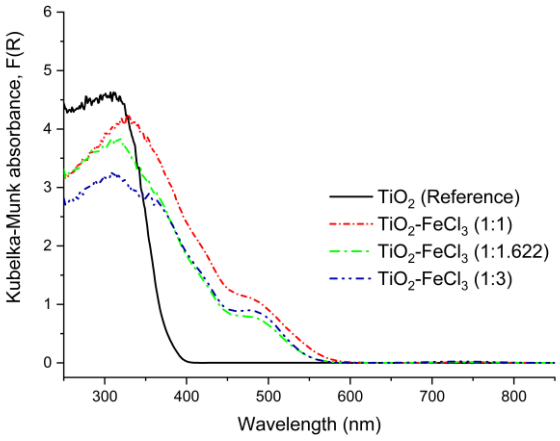

Figure 2 - Kubelka–Munk function of the undoped TiO_2 (reference) and TiO_2 with $FeCl_3$ with the different concentrations.

For longer wavelength, these absorption edge shifts are due to the appearance of iron in the doping process which in turn reduces the energy band (E_g) aperture of TiO_2, and thus extend the use for visible light, as previously predicted.
In Figure 3, the Kubelka-Munk transformation values versus Energy (eV) can be seen. The E_g was calculated by drawing a tangent line to the inflection point on the curve, which is indicated on the horizontal axis by the value of the tangent line.
Thus, it can be seen that the E_g value for the undoped TiO_2 (3.16 eV) is clearly higher than the $FeCl_3$ doped TiO_2 at different concentrations. The E_g values were always the lower for the other concentrations studied, i.e., (1:1), (1:1.622), and (1:3) thus presenting Eg values of 2.08, 2.21, and 2.06 eV, respectively.

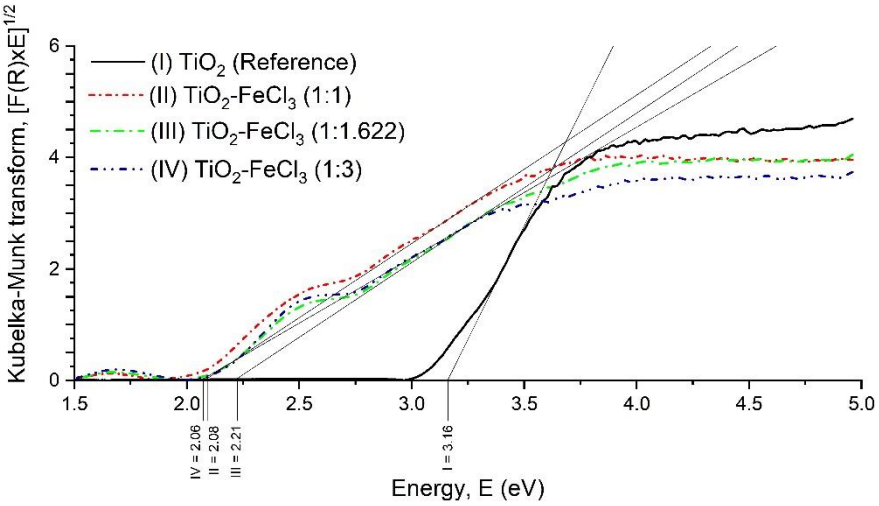

Figure 3 - Results of Kubelka–Munk transform vs Energy, E (eV) of the light absorbed for the undoped TiO_2 (reference) and doped TiO_2 with $FeCl_3$ with the different concentrations.

Incorporation of $FeCl_3$ into the TiO_2 lattice causes a decrease in the energy band gaps and, this may improve the photocatalytic performance due to the activation of TiO_2 in the visible region of the electromagnetic spectrum [12].

3.2 *X-ray diffraction (XRD)*
To study the crystalline phase of each doped material, X-ray diffraction (XRD) patterning was used. Figure 4 shows the XRD patterns of the TiO_2 nanoparticles (undoped) at various concentrations of TiO_2-$FeCl_3$. Also, the existence of both anatase and rutile phases are indicated in the figure.
The comparison of the results of the samples with TiO_2-$FeCl_3$, shows that there are no significant differences between their pattern and the XRD pattern of reference TiO_2 nanoparticles. The fraction of the anatase phase of doped TiO_2 nanoparticles has the same magnitude as the reference TiO_2 particles and, consequently, doping has no significant influence on the anatase-to-rutile transformation (ART).

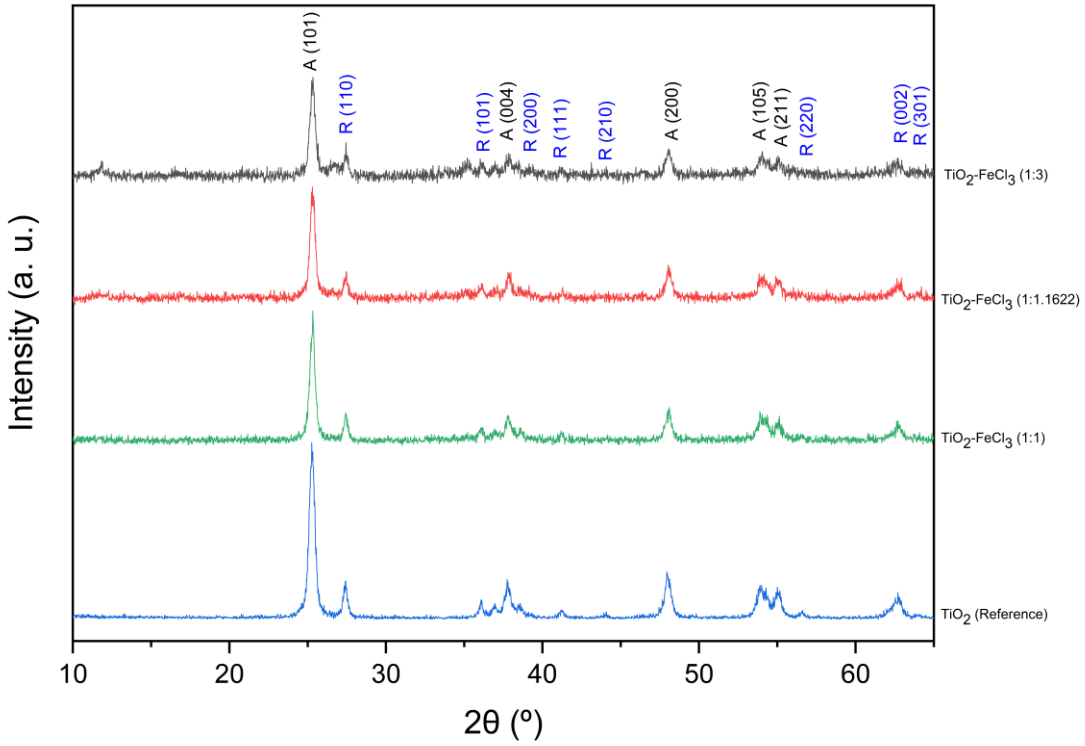

Figure 4 - X-ray diffraction patterns of doped TiO_2 nanoparticle.

3.3 *Fourier-Transform Infrared Spectroscopy (FTIR)*

To analyze the chemical composition of the doped materials, Fourier-Transform Infrared Spectroscopy (FTIR) analysis was performed for the vibration bands in the wavenumber range of 400 – 4000 cm^{-1}. Figure 5 shows the FTIR spectrum of undoped TiO_2 (reference), undoped $FeCl_3$ (reference), and doped TiO_2 at various concentrations with $FeCl_3$.

The peaks 3390 and 3323 cm^{-1} are related to H-O-H vibrational bonding, and the peaks at 1600 and 1550 cm^{-1} are indexed to -OH vibrational bonds, both indicating the presence of absorbed hydroxyl groups in the samples. The groups containing oxygen play an effective role in photocatalytic activity and thus are able to generate more hydroxyl radicals. The increase in hydroxyl group bonds related to the doping process may be related to the fact that this process involves aqueous solutions and aqueous dispersions, even after the oven drying process, as recommended in the literature. The peak at 2280 cm^{1} signals for the Ti-O-Fe vibration, which is a very intense bond from the doping process [19]. The peaks shown in the range of 528-458 cm^{-1} are due to the Ti-O group [20]. In the spectrum of undoped TiO_2 (reference), the peaks in the region of 650-1200 cm^{-1} can be attributed to the Ti-O-Ti bond and the Ti-O-Fe stretching vibration. In the case of Fe-doped TiO_2 peaks, in the region of 500-1200 cm^{-1}, the peak at 1120 cm^{-1}, is assigned to the O-Ti-O vibration and the Fe-O-Fe symmetric stretching vibration. On the other hand, the peaks observed at 625 cm^{-1} prove the existence of iron oxyhydroxide Fe-O-OH. Below 1000 cm^{-1}, Fe-O and Ti-O bending frequency overlap may occur due to the similarity between the peak values of the respective chemical bonds. All the chemical bonds present in the doped material and their wavelength are summarized in Table 1.

Table 1 - Chemical bonds and their functional groups.

Wavenumber (cm^{-1})	**Functional group assigned**
3323	Vibration bond H-O-H
1600	Vibration bond -OH
2280	Ti-O-Fe vibration
1120	O-Ti-O vibration and the symmetric Fe-O-Fe stretching vibration
458	Ti-O

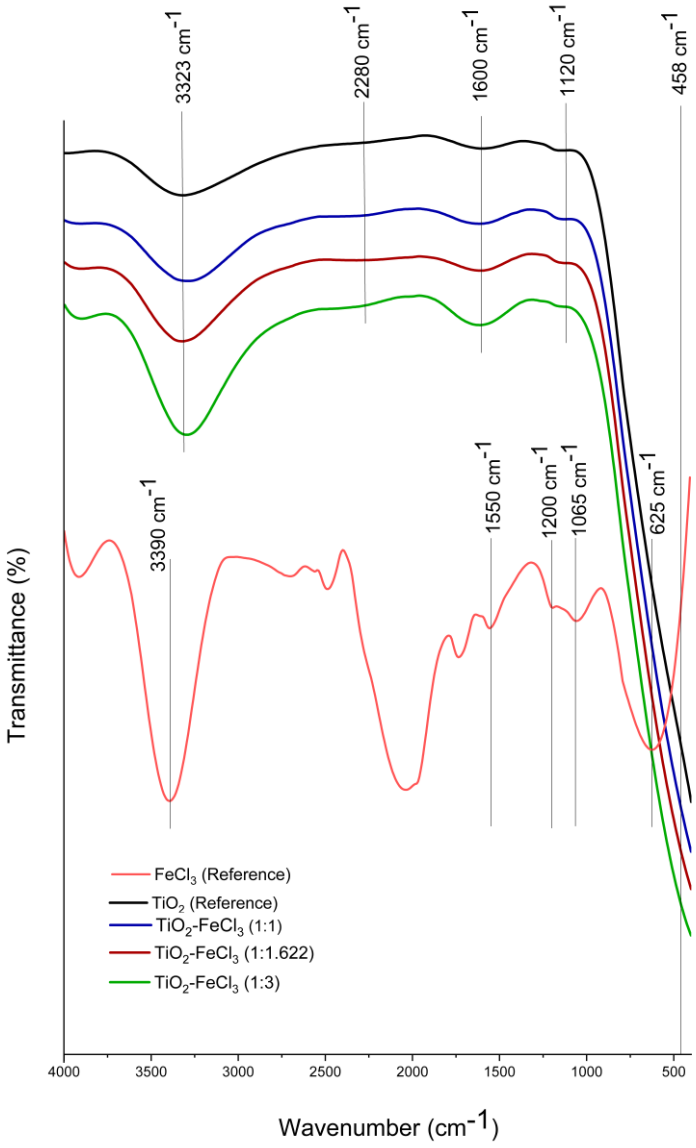

Figure 5 - FTIR spectra for the TiO_2 (reference), $FeCl_3$ (reference), and the different concentrations of doped TiO_2 with $FeCl_3$.

3.4 *Scanning Electron Microscopy (SEM)*

Scanning Electron Microscopy (SEM) was used to investigate the homogenization and dispersion of the samples. The samples selected for the respective analysis were undoped TiO_2 (reference), $FeCl_3$ doped TiO_2 at concentrations (1:1.622) and (1:3). This test will help to assess the morphological effect of the increasing concentration of $FeCl_3$.

In Figure 6, the agglomeration of TiO_2 particles can be identified. The nanoparticles tend to agglomerate into clusters because the nanoparticles are irregularly shaped and randomly distributed. Also, their nanometer scale size can be checked, ranging from 20 to 30 nanometers. Figure 7 (a) and (b) show the micrograph and corresponding spectrum of TiO_2 doped with $FeCl_3$ at the concentrations of (1:1.622) and (1:3), respectively. It can be inferred that after the doping process, iron is present in the sample, and the particle size remains similar to the reference TiO_2. Since the TiO_2 and Fe particles cannot be observed separately, there are indications that iron is homogeneously distributed in TiO_2, which may have occurred a chemical reaction between them in the doping process becoming a single particle, and the particle sizes remain with the same magnitude as the TiO_2 (reference) particles.

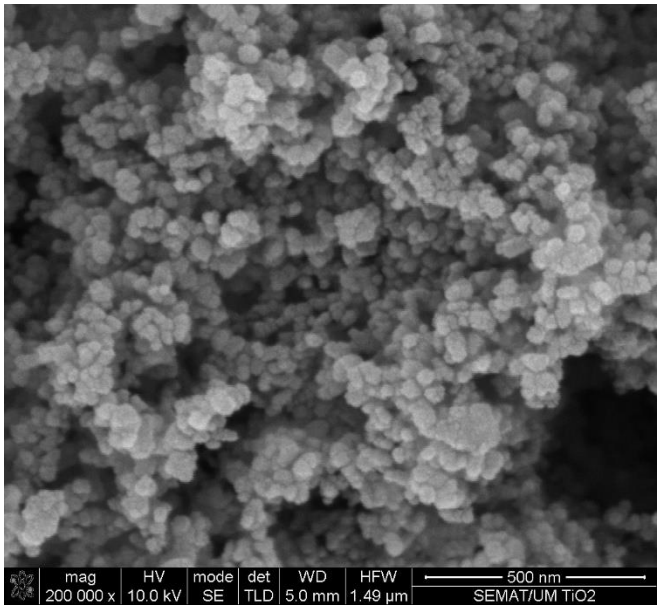

Figure 6- SEM micrograph representation for TiO_2 (reference).

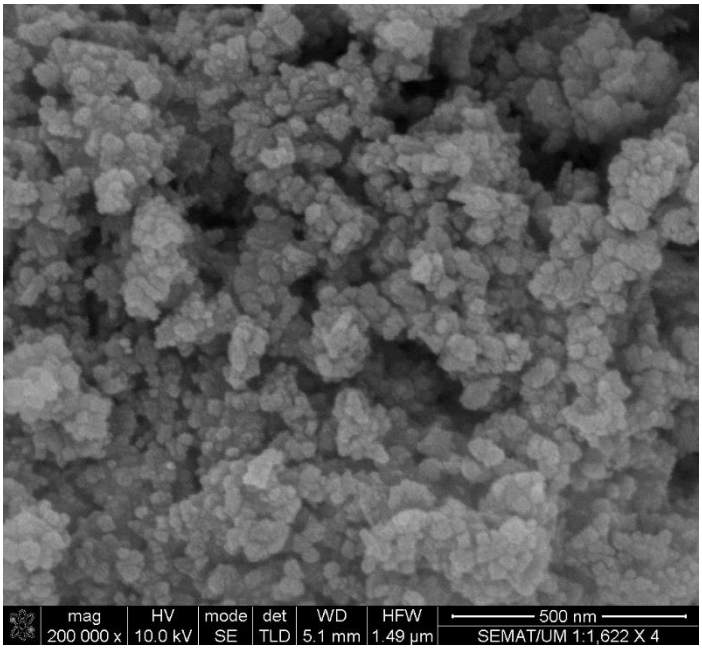

(a)

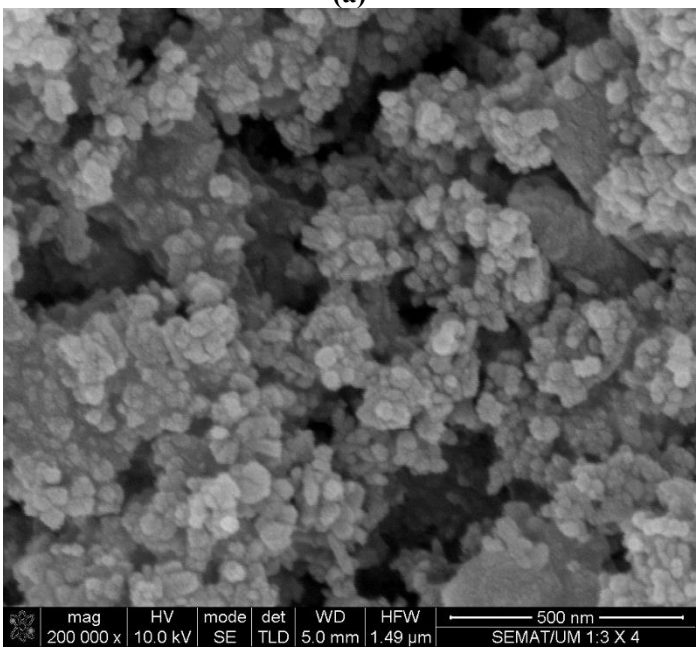

(b)

Figure 7 - SEM micrograph representation for TiO_2-$FeCl_3$ in concentrations (a) 1:1.622 and (b) 1:3.

4. Conclusions

This research work evaluated the doping process of TiO_2 semiconductor nanoparticles in order to activate photocatalysis using $FeCl_3$ under visible light and consequently improve the capture of pollutants present in the atmosphere. The following conclusions can be drawn from the results:

- The light absorption measurements and the parameters determined by the Kubelka-Munk transformation showed that the process of doping TiO_2 with $FeCl_3$ shifted the absorption edge to longer wavelength values, causing changes in the optical properties of the material. Furthermore, for the different concentrations of TiO_2-$FeCl_3$, the E_g value decreased compared to the E_g of undoped TiO_2 (reference).
- The XRD analysis shows that the nanoparticles have no significant influence on the anatase-to-rutile transformation (ART), compared to undoped TiO_2 (reference).
- The FTIR analysis showed that the Fe-doping process changes the spectrum of the reference TiO_2, especially with regard to the higher intensity of hydroxyl bonds and peaks indicating the vibration of the Ti-O-Fe bond.
- The SEM analysis shows that the particles are within the nanometer scale, and that there are indications of the chemical reaction may have occurred between TiO_2 and Fe in the doping process.

As a general conclusion, there are good indications that the incorporation of iron, through the doping process in TiO_2 nanoparticles will improve their photocatalytic activity.

As next steps of this investigation, the doped TiO_2 will undergo a calcination process in the various concentrations of TiO_2-$FeCl_3$. Subsequently, the doped and calcined powders will be evaluated by X-ray diffraction (XRD) to identify in detail the crystalline phase of each doped material, regarding the average crystal size, lattice parameters and the anatase phase content ratio. Finally, the best doped-TiO_2 will be performed by X-ray Photoelectron Spectroscopy (XPS) in order to analyze its elemental composition (chemical and electronic states), and verify whether exists bonds between Fe and TiO_2.

Acknowledges

This work has been supported by the Portuguese Foundation for Science and Technology (FCT) under the framework of the Strategic Funding UIDB/04650/2020, UIDB/04029/2020, and NanoAir PTDC/FIS-MAC/6606/2020.

References

[1] Zabihi-Mobarakeh, H.; Nezamzadeh-Ejhieh, A. Application of supported TiO2 onto Iranian clinoptilolite nanoparticles in the photodegradation of mixture of aniline and 2, 4-dinitroaniline aqueous solution. *J. Ind. Eng. Chem.* **2015**, *26*, 315–321, doi:10.1016/j.jiec.2014.12.003.

[2] Nezamzadeh-Ejhieh, A.; Bahrami, M. Investigation of the photocatalytic activity of supported ZnO–TiO 2 on clinoptilolite nano-particles towards photodegradation of wastewater-contained phenol. *Desalin. Water Treat.* **2015**, *55*, 1096–1104, doi:10.1080/19443994.2014.922443.

[3] Rocha Segundo, I.; Freitas, E.; Landi Jr, S.; Costa, M.F.M.; Carneiro, J.O. Smart, Photocatalytic and Self-Cleaning Asphalt Mixtures: A Literature Review. *Coatings* **2019**, *9*, doi:10.3390/coatings9110696.

[4] Carneiro, J.O.; Azevedo, S.; Fernandes, F.; Freitas, E.; Pereira, M.; Tavares, C.J.; Lanceros-Méndez, S.; Teixeira, V. Synthesis of iron-doped TiO2 nanoparticles by ball-milling process: the influence of process parameters on the structural, optical, magnetic, and photocatalytic properties. *J. Mater. Sci.* **2014**, *49*, 7476–7488, doi:10.1007/s10853-014-8453-3.

[5] Ghorbanpour, M.; Feizi, A. Iron-doped TiO2 Catalysts with Photocatalytic Activity. *J. Water Environ. Nanotechnol.* **2019**, *4*, 60–66, doi:10.22090/JWENT.2019.01.006.

[6] Etacheri, V.; Di Valentin, C.; Schneider, J.; Bahnemann, D.; Pillai, S.C. Visible-light activation of TiO2 photocatalysts: Advances in theory and experiments. *J. Photochem. Photobiol. C Photochem. Rev.* **2015**, *25*, 1–29, doi:10.1016/j.jphotochemrev.2015.08.003.

[7] Rocha Segundo; Freitas; Landi Jr.; Costa; Carneiro Smart, Photocatalytic and Self-Cleaning Asphalt Mixtures: A Literature Review. *Coatings* **2019**, *9*, 696, doi:10.3390/coatings9110696.
[8] Venturini, L.; Bacchi, I. Research, Design and Development of a Photocatalytic Asphalt Pavement. *Proc. 2nd Int. Conf. Environ. Friendly Roads ENVIROAD* **2009**, 1–16.
[9] Zaleska, A. Doped-TiO2: A Review. *Recent Patents Eng.* **2008**, *2*, 157–164, doi:10.2174/187221208786306289.
[10] Cao, X.; Yang, X.; Li, H.; Huang, W.; Liu, X. Investigation of Ce-TiO2 photocatalyst and its application in asphalt- based specimens for NO degradation. *Constr. Build. Mater.* **2017**, *148*, 824–832, doi:10.1016/j.conbuildmat.2017.05.095.
[11] Piątkowska, A.; Janus, M.; Szymański, K.; Mozia, S. C-,N- and S-Doped TiO2 Photocatalysts: A Review. *Catalysts* **2021**, *11*, 144, doi:10.3390/catal11010144.
[12] Eadi, S.B.; Kim, S.; Jeong, S.W.; Jeon, H.W. Novel Preparation of Fe Doped TiO 2 Nanoparticles and Their Application for Gas Sensor and Photocatalytic Degradation. *Adv. Mater. Sci. Eng.* **2017**, *2017*, 1–6, doi:10.1155/2017/2191659.
[13] Landi, S.; Carneiro, J.; Soares, O.S.G.P.; Pereira, M.F.R.; Gomes, A.C.; Ribeiro, A.; Fonseca, A.M.; Parpot, P.; Neves, I.C. Photocatalytic performance of N-doped TiO2nano-SiO2-HY nanocomposites immobilized over cotton fabrics. *J. Mater. Res. Technol.* **2019**, *8*, 1933–1943, doi:10.1016/j.jmrt.2018.06.025.
[14] Adamek, E.; Baran1, W.; Ziemiańska, Justyna Makowski1, A.; Sobczak1, A. Use of a TiO2/FeCl3 mixture in environmental cleaning technology. In; 2012; Vol. 6(2).
[15] Fan, W.; Chan, K.Y.; Zhang, C.; Zhang, K.; Ning, Z.; Leung, M.K.H. Solar photocatalytic asphalt for removal of vehicular NOx: A feasibility study. *Appl. Energy* **2018**, *225*, 535–541, doi:10.1016/j.apenergy.2018.04.134.
[16] Tang, B.; Liu, X.; Huang, W.; Cao, X. Preparation of La-doped nanometer TiO2 and its application for NO removal on asphalt concrete. *Road Mater. Pavement Des.* **2017**, *18*, 43–53, doi:10.1080/14680629.2017.1329860.
[17] Valencia, S.; Marin, J.M.; Restrepo, G. Study of the Bandgap of Synthesized Titanium Dioxide Nanoparticules Using the Sol-Gel Method and a Hydrothermal Treatment. *Open Mater. Sci. J.* **2010**, *4*, 9–14, doi:10.2174/1874088X01004020009.
[18] Kisch, H.; Sakthivel, S.; Janczarek, M.; Mitoraj, D. A Low-Band Gap, Nitrogen-Modified Titania Visible-Light Photocatalyst. *J. Phys. Chem. C* **2007**, *111*, 11445–11449, doi:10.1021/jp066457y.
[19] Shahmoradi, B.; Maleki, A.; Byrappa, K. Removal of Disperse Orange 25 using in situ surface-modified iron-doped TiO 2 nanoparticles. *Desalin. Water Treat.* **2015**, *53*, 3615–3622, doi:10.1080/19443994.2013.873994.
[20] Marami, M.B.; Farahmandjou, M.; Khoshnevisan, B. Sol–Gel Synthesis of Fe-Doped TiO2 Nanocrystals. *J. Electron. Mater.* **2018**, *47*, 3741–3748, doi:10.1007/s11664-018-6234-5.